Supporting Information

Metal-organic framework derivatives with gradient structure via multidimensional assembly engineering for tunable efficient microwave absorption

Zhe Zhang[a], Jiewu Cui[a,*], Dongbo Yu[a], Pengjie Zhang[b], Yong Zhang[a], Song Ma[c], Wei Sun[b], Xiaohui Liang[d], Yucheng Wu[a,*]

[a.] School of Materials Science and Engineering, Key Laboratory of Advanced Functional Materials and Devices of Anhui Province, Hefei University of Technology, Hefei 230009, P. R. China

[b.] BGRIMM Technology Group Co, Ltd, Beijing 102600, P. R. China

[c.] Shenyang National Laboratory for Materials Science, Institute of Metal Research, Chinese Academy of Sciences, Shenyang 110016, P. R. China

[d.] Hangzhou Dianzi University, Hangzhou 310018, P. R. China

Corresponding author: Jiewu Cui (jwcui@hfut.edu.cn), Yucheng Wu (ycwu@hfut.edu.cn)

Experimental section

Materials

1,3,5–Benzenetricarboxylic acid (H_3BTC), 2,5–dihydroxyterephthalic acid (H_4dobdc), Cobalt(II) acetate tetrahydrate ($(CH_3COO)_2Co·4H_2O$), Cobalt(II) chloride hexahydrate ($CoCl_2·6H_2O$), Cobalt(II) nitrate hexahydrate ($Co(NO_3)_2·6H_2O$), Sodium hydroxide (NaOH), 2–methylimidazole (Hmim), ethanol, methanol, N,N–dimethylformamide (DMF) were obtained from Sinopharm Chemical Reagent Co., Ltd. All chemicals do not require further purification. Deionized water produced directly by our laboratory (electrical resistivity ~ 18.2 MΩ·cm).

Synthesis of Co–BTC nanowires and Co–BTC@ZIF–67

For the synthesis of Co–BTC nanowires, 535.5 mg of $(CH_3COO)_2Co·4H_2O$ was first dissolved in 10 ml of deionized water, then 420.3 mg of 1,3,5–benzenetricarboxylic acid was dissolved in 90 ml of deionized water, followed by the reaction of the two precursor solutions with magnetic stirring at 100 °C for 15 min. The pink precipitate was collected by centrifugation, washed with ethanol, and dried in an oven at 60°C for 24. Subsequently, 140 mg of the prepared Co–BTC nanowires were dispersed in Hmim methanol solution (500 mg Hmim (15 ml methanol)), followed by dropwise addition of $Co(NO_3)_2·6H_2O$ methanol solution (300 mg $Co(NO_3)_2·6H_2O$ (10 ml methanol)). React for 20 min, centrifuged to extracted the purple precipitate, washed with ethanol, and dried in an oven at 60 °C for 24 h to finally prepare Co–BTC@ZIF–67.

Synthesis of Co–MOF–74 nanorods and Co–MOF–74@ZIF–67

For the synthesis of Co–MOF–74 nanorods, 951.7 mg of $CoCl_2 \cdot 6H_2O$ were first dissolved in 10 ml of deionized water, then 396.3 mg of DHTA and 180 mg of NaOH were dispersed in 90 ml of deionized water, followed by the reaction of the two precursor solutions with magnetic stirring for 1 h at 100 °C. The brownish–yellow precipitate was collected by centrifugation, washed with ethanol, and dried in an oven at 60 °C for 24 h. Then, 40 mg of the prepared Co–MOF–74 nanorods were dispersed in Hmim methanol solution (500 mg Hmim (5 ml methanol)), followed by dropwise addition of $Co(NO_3)_2 \cdot 6H_2O$ methanol solution (25 mg $Co(NO_3)_2 \cdot 6H_2O$ (10 ml methanol)). React for 20 min, centrifuged to collect the brownish–purple precipitate, washed with ethanol, and dried in an oven at 60 °C for 24 h to finally obtain Co–MOF–74@ZIF–67.

Synthesis of Nanowire/Nanorod@bubble

For the synthesis of Nanowire/Nanorod@bubble, 60/30 mg of H_4dobdc were dissolved in 40 ml of DMF and add 50 mg Co–BTC@ZIF–67/Co–MOF–74@ZIF–67 to make a homogeneous suspensions. Transfer suspensions to 50 ml Teflon–lined stainless–steel autoclaves and heat at 110 °C for 12 h. The precipitates obtained were collected by centrifugation, washed with ethanol and dried in an oven at 60 °C for 24 h.

Synthesis of carbon matrix composites derived from MOF precursors

The previously synthesized MOF precursors included Co–BTC, Co–MOF–74, Co–BTC@ZIF–67, Co–MOF–74@ZIF–67, Nanowire@bubble, and Nanorod@bubble. The above precursors were pyrolyzed in an Ar atmosphere at 700

°C for 2 h at a heating rate of 2 °C/min, and the black powder obtained was collected after natural cooling to room temperature. The obtained products were marked as Co–BTC–C, Co–MOF–74–C, Co–BTC@ZIF–67–C, Co–MOF–74@ZIF–67–C, Nanowire@bubble–C, and Nanorod@bubble–C, respectively.

Characterization

The crystal structures of the prepared samples were characterized by X–ray diffractometry (XRD, Rigaku D/MAX2500VL/PC) with Cu–Kα radiation. The Raman spectrum of the samples were measured using a micro confocal laser Raman spectrometer (LabRAM HR Evolution) with a laser wavelength of 532 nm. Surface chemistry of samples analyzed by X–ray photoelectron spectroscopy (XPS, ESCALAB 250Xi) equipped with a monochromatic Al Kα. The morphology, microstructure and elemental distribution of the samples prepared were characterized using field–emission scanning electron microscopy (FESEM, Regulus 8230), transmission electron microscopy (TEM, JEM–1400flash), field–emission transmission electron microscopy (FETEM, Talos F200X G2) with energy dispersive X–rays spectroscopy (EDX). The specific surface area and pore size distribution of the samples were collected at 77 K by a physisorption analyzer (Autosorb–IQ3). The room temperature magnetic characteristics of the samples were investigated by a vibrating sample magnetometer (VSM, LakeShore 7404).

Microwave Absorption Measurements

The prepared Co–BTC–C, Co–MOF–74–C, Co–BTC@ZIF–67–C, Co–MOF–74@ZIF–67–C, Nanowire@bubble–C, and Nanorod@bubble–C powder were mixed

uniformly with paraffin wax at a mass ratio of 25:75 and molded into coaxial rings (outer diameter: 7.00 mm, inner diameter: 3.04 mm). The electromagnetic parameters in the frequency range of 2–18 GHz were measured on a network vector analyzer (ROHDE&SCHWARZ ZNA43) using the coaxial line method.

Radar Cross Section (RCS) Simulation

Radar cross–section (RCS) were simulated through CST Studio Suite 2019 to evaluate scattering ability of Co–BTC–C, Co–MOF–74–C, Co–BTC@ZIF–67–C, Co–MOF–74@ZIF–67–C, Nanowire@bubble–C, Nanorod@bubble–C composites for electromagnetic waves under the far field. All samples were modeled for simulation as two double–layer composite plates consisting of a perfect electrical conductor (PEC) (200 mm * 200 mm) and an absorber layer (200 mm * 200 mm). The Co–BTC–C, Co–BTC@ZIF–67–C, Nanowire@bubble–C absorber layer thicknesses are all set to 2.44 mm at 9.4 GHz. The Co–MOF–74–C, Co–MOF–74@ZIF–67–C, Nanorod@bubble–C absorber layer thicknesses are all set to 1.97 mm at 13.92 GHz. Models were placed on the XOY plane to receive incoming electromagnetic waves from the negative direction of Z–axis. Using the open (with space) boundary conditions in this direction, the scattering direction is determined by θ and φ. The RCS value can be calculated by the following equation [1]:

$$\sigma(dB\ m^2) = 10\log\left(\frac{4\pi S}{\lambda^2}\left|\frac{E_s}{E_i}\right|^2\right) = 10\log\left(\frac{4\pi S}{\lambda^2}\left|\frac{H_s}{H_i}\right|^2\right)$$

where, *S* and λ are the area of simulation model and wavelength of electromagnetic wave, *Es* and *Ei* represent intensity of scattered electric field and intensity of incident electric field, *Hs* and *Hi* represent intensity of scattering magnetic field and incident

magnetic field strength.

Equations

The reflection loss (RL) values can be calculated according on the transmission line theory by equation S1 and equation S2 [2].

$$Z_{in} = Z_0\sqrt{\mu_r/\varepsilon_r}\tan\left[j(2\pi f d/c)\sqrt{\mu_r\varepsilon_r}\right] \quad \text{(S1)}$$

$$RL(dB) = 20\log\left|(Z_{in} - Z_0)/(Z_{in} + Z_0)\right| \quad \text{(S2)}$$

where, Z_0, Z_{in}, c, d, and f represent the impedance of free space, the input impedance of absorber, the velocity of light, the thickness of absorber and the frequency of the microwave, respectively. ε_r and μ_r represent the complex permittivity and complex permeability.

Based on the Debye theory, the Cole-Cole curve (ε'' vs. ε') can be used to demonstrate the polarization relaxation process within the absorber [3]. If the Cole-Cole curve presents complete semicircles, it indicates the presence of Debye relaxation processes within the material.

$$(\varepsilon' - \frac{\varepsilon_s + \varepsilon_\infty}{2})^2 + (\varepsilon'')^2 = \left(\frac{\varepsilon_s - \varepsilon_\infty}{2}\right)^2 \quad \text{(S3)}$$

where, ε_S and ε_∞ represent the static permittivity and the relative permittivity at infinite frequency.

If the magnetic loss is caused only by eddy current loss, the calculated eddy current coefficient (C_0) should remain constant even if the frequency rises, according to the following equation S4 [4].

$$C_0 = \mu''(\mu')^{-2}f^{-1} \quad \text{(S4)}$$

Interference phase cancellation loss is also a key factor that enhances and

influences the absorption of electromagnetic waves in absorbers. When the thickness of the absorber satisfies the theoretical thickness of the quarter-wavelength model, the incident and reflected waves will phase cancel at the interface with a 180° phase difference. And this can be described using the quarter-wavelength model theory [5, 6]:

$$t_m = \frac{(2m-1)\lambda}{4} = \frac{(2m-1)c}{4nf}\,(m = 1, 2, 3\cdots) \quad \text{(S5)}$$

where λ, c, t_m and f represent the wavelength, the velocity of light, the matching thickness, and the matching frequency, and n. is the refractive index, which is the real part of the square root of the product of complex permittivity and complex permeability.

The attenuation constant (α) can comprehensively evaluate the ability to attenuate electromagnetic waves within an absorber [7].

$$\alpha = \frac{\sqrt{2}\pi f}{c}\sqrt{\left(\mu''\varepsilon'' - \mu'\varepsilon'\right) + \sqrt{\left(\mu''\varepsilon'' - \mu'\varepsilon'\right)^2 + \left(\mu'\varepsilon'' + \mu''\varepsilon'\right)^2}} \quad \text{(S6)}$$

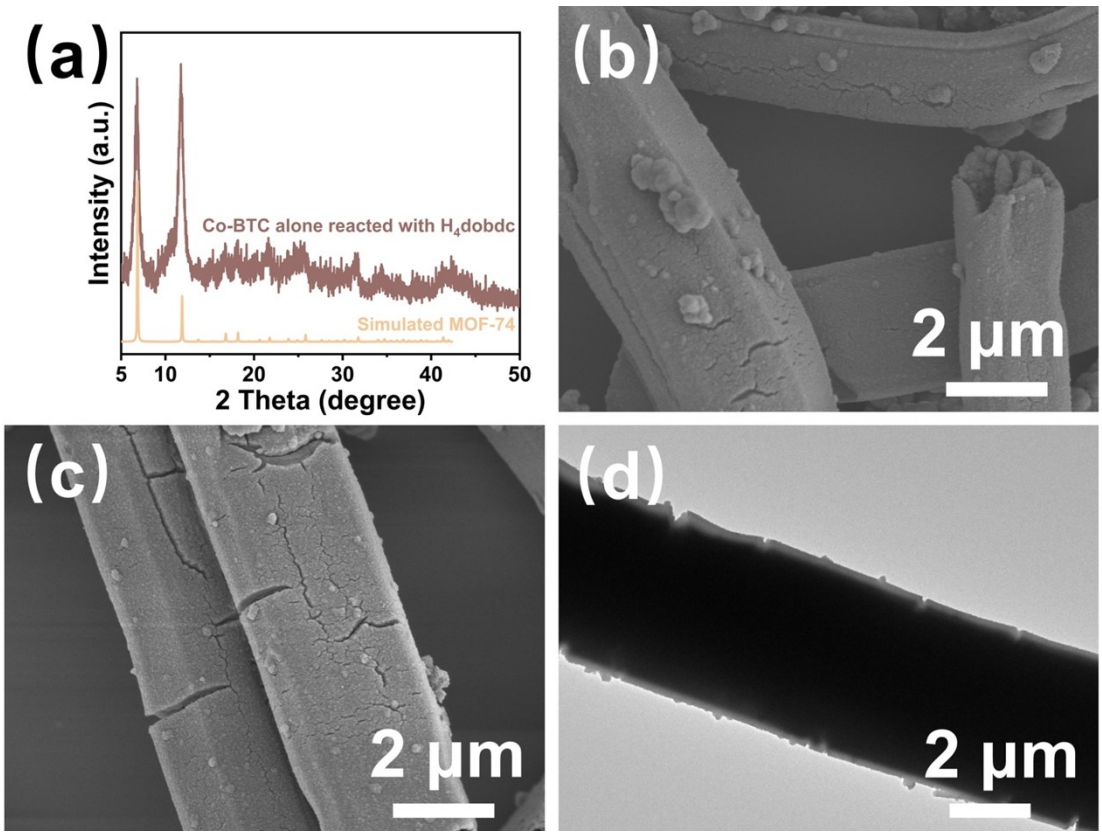

Figure S1. a) XRD patterns, b–c) SEM images, and d) TEM image of Co–BTC alone reacted with H_4dobdc.

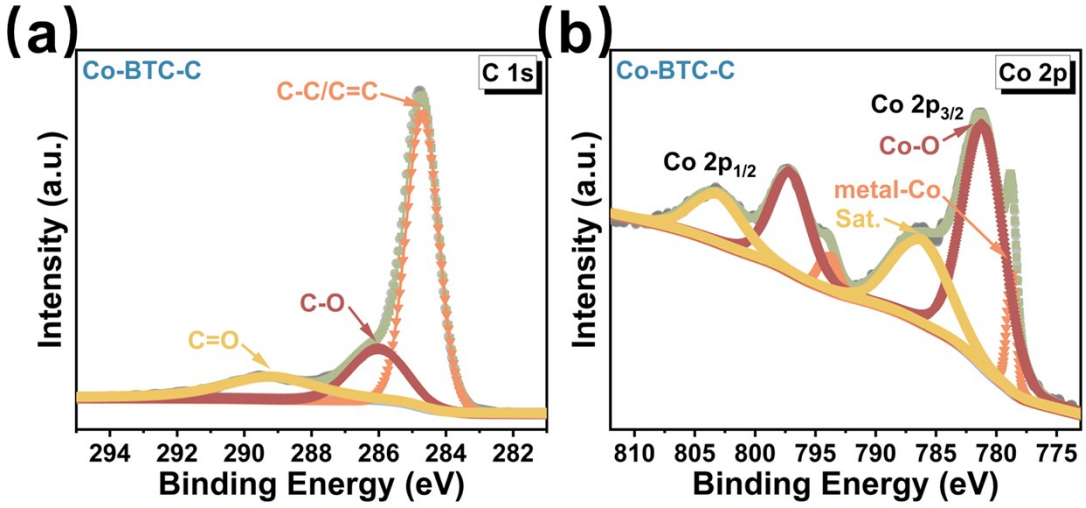

Figure S2. a) C 1s spectra, b) Co 2p spectra of Co–BTC–C.

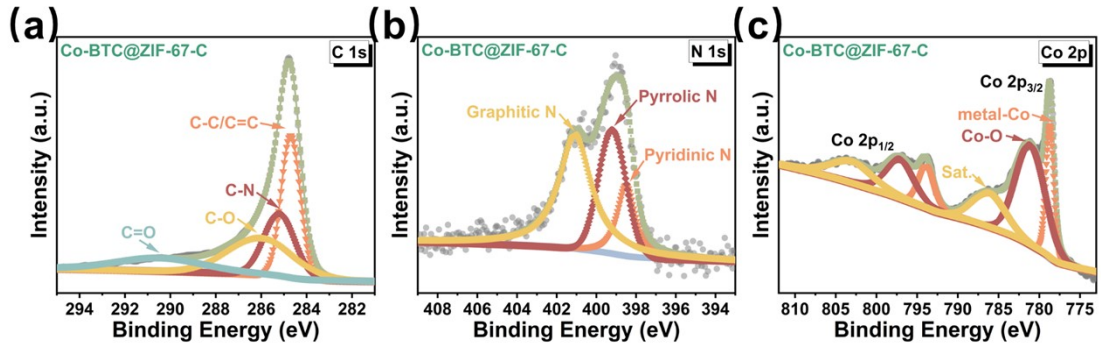

Figure S3. a) C 1s spectra, b) N 1s spectra, and c) Co 2p spectra of Co–BTC@ZIF–67–C.

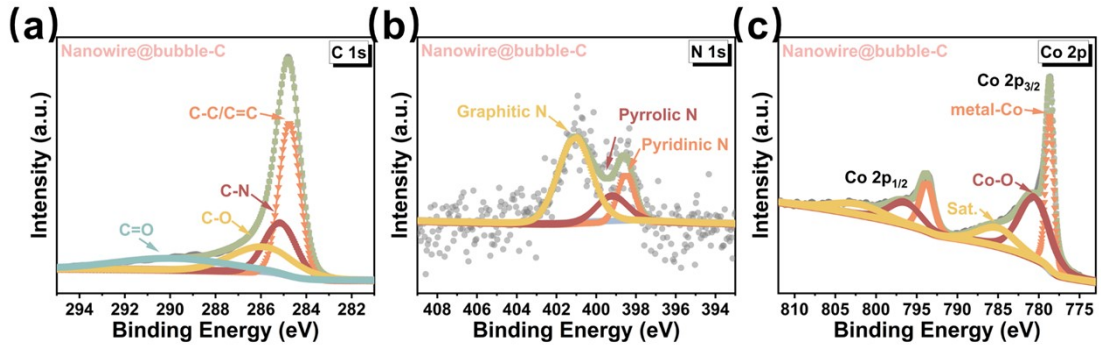

Figure S4. a) C 1s spectra, b) N 1s spectra, and c) Co 2p spectra of Nanowire@bubble–C.

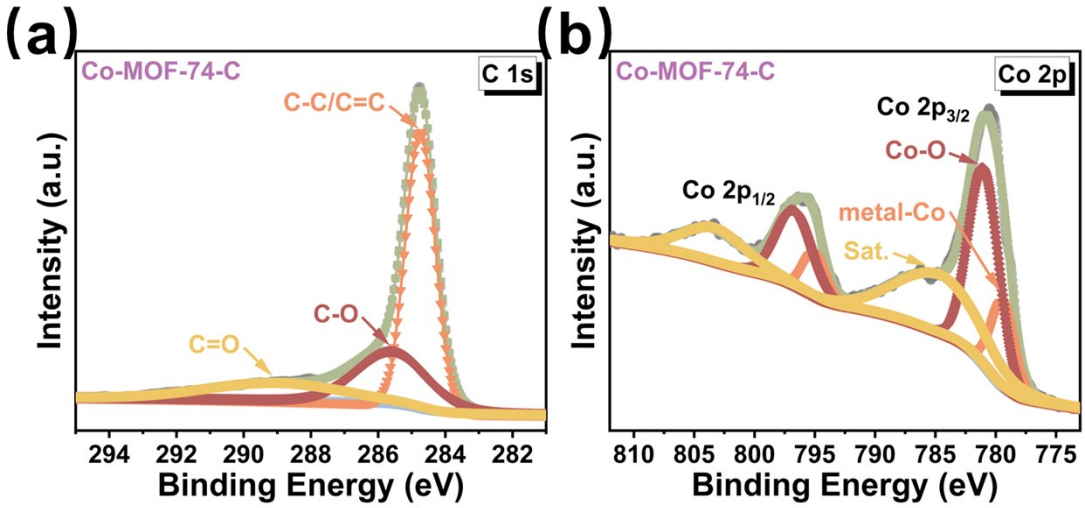

Figure S5. a) C 1s spectra, b) Co 2p spectra of Co–MOF–74–C.

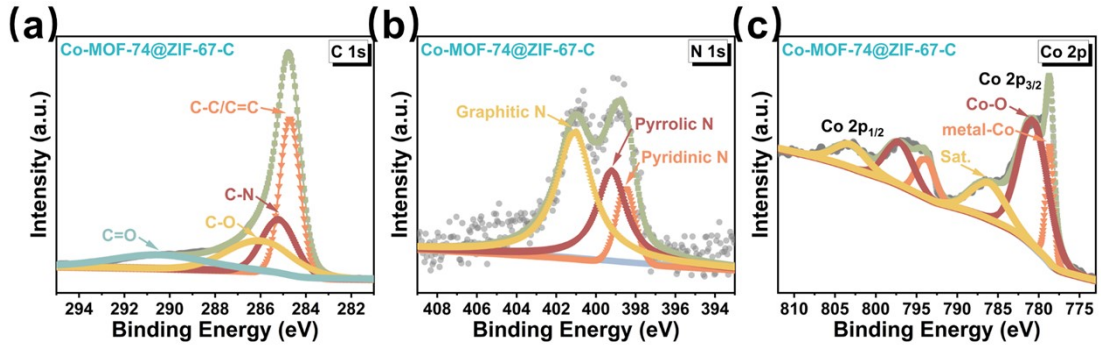

Figure S6. a) C 1s spectra, b) N 1s spectra, and c) Co 2p spectra of Co–MOF–74@ZIF–67–C.

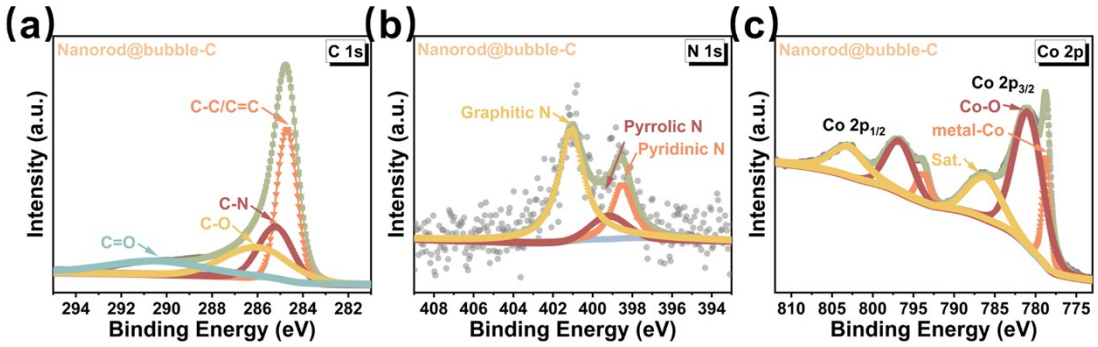

Figure S7. a) C 1s spectra, b) N 1s spectra, and c) Co 2p spectra of Nanorod@bubble–C.

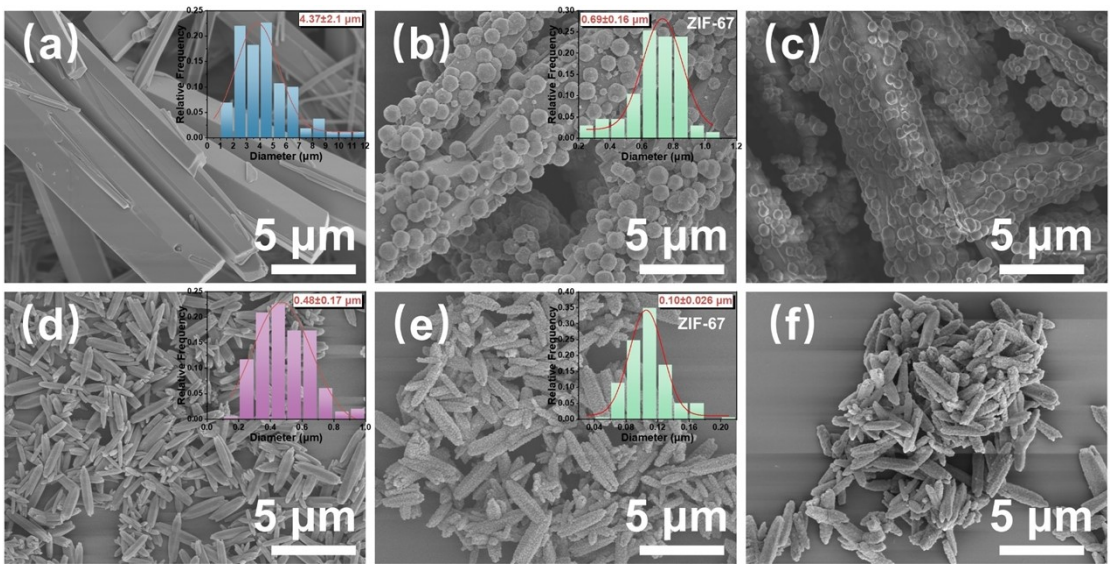

Figure S8. a) SEM image of Co–BTC (inset is diameter distribution of Co–BTC), b) SEM image of Co–BTC@ZIF–67 (inset is diameter distribution of ZIF–67 particles), c) SEM image of Nanowire@bubble. d) SEM image of Co– Co–MOF–74 (inset is diameter distribution of Co–MOF–74), e) SEM image of Co–MOF–74@ZIF–67 (inset is diameter distribution of ZIF–67 particles), f) SEM image of Nanorod@bubble.

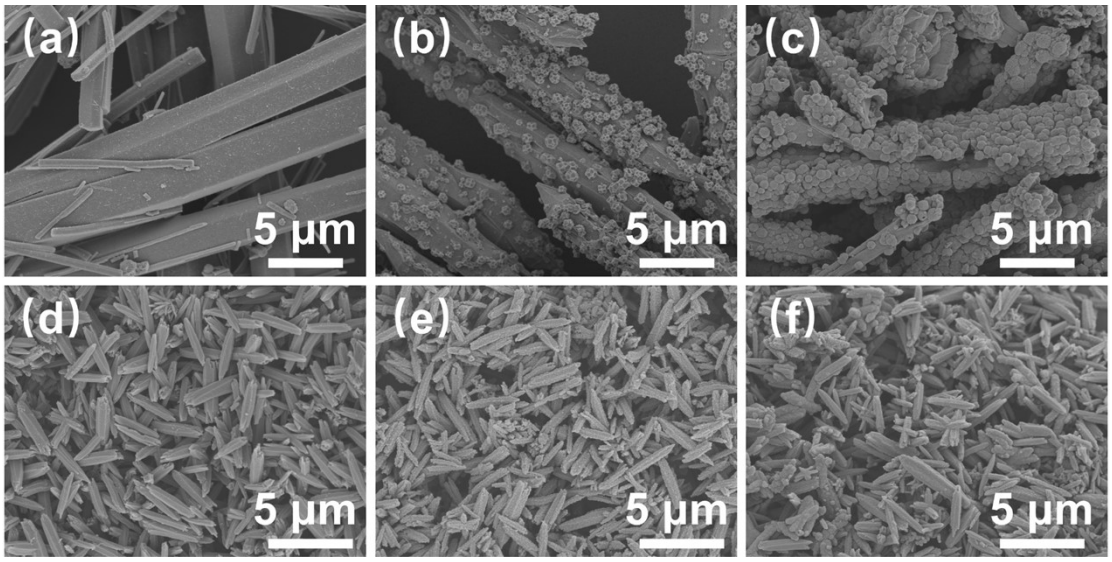

Figure S9. a–c) SEM images of Co–BTC–C, Co–BTC@ZIF–67–C, and Nanowire@bubble–C. d–f) SEM images of Co–MOF–74–C, Co–MOF–74@ZIF–67–C, and Nanorod@bubble–C.

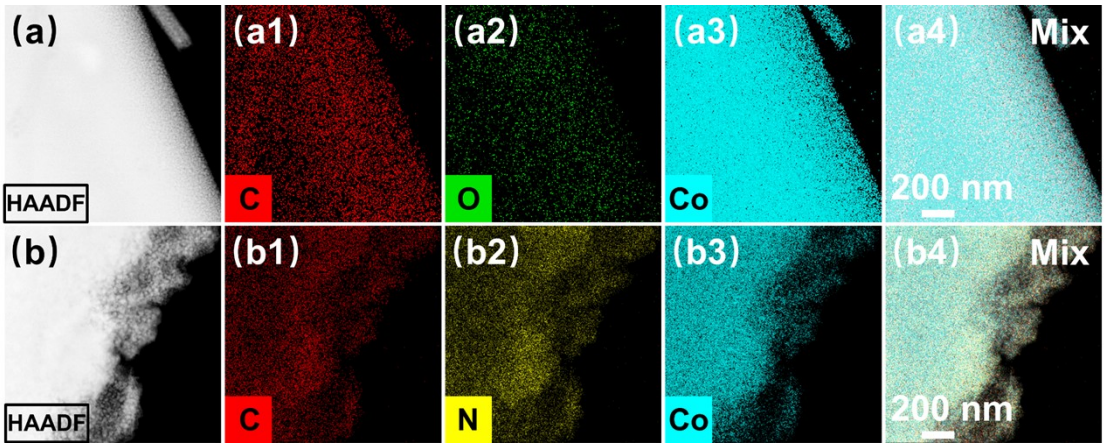

Figure S10. a) HAADF–STEM image and a1–a4) EDX mapping images of Co–BTC–C. b) HAADF–STEM image and b1–b4) EDX mapping images of Co–BTC@ZIF–67–C.

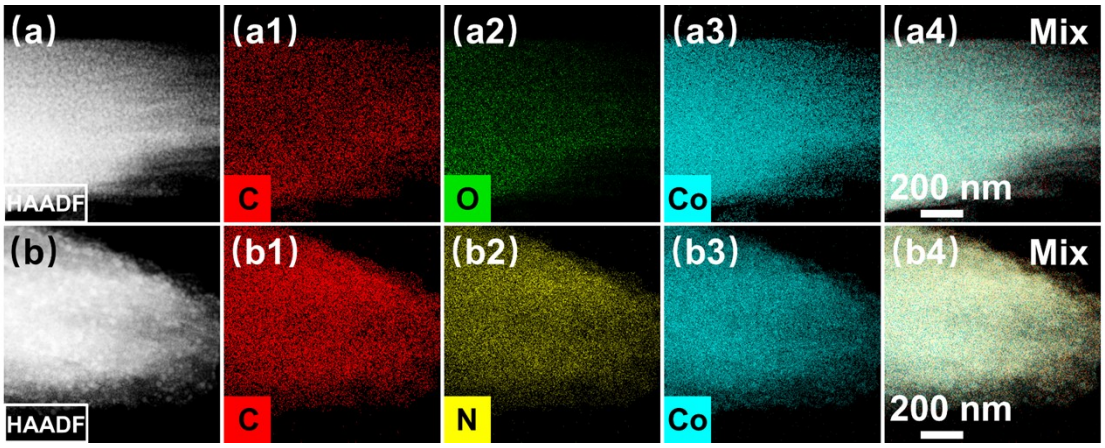

Figure S11. a) HAADF–STEM image and a1–a4) EDX mapping images of Co–MOF–74–C. b) HAADF–STEM image and b1–b4) EDX mapping images of Co–MOF–74@ZIF–67–C.

(a) Co-BTC-C

Z	Element	Atomic Fraction (%)	Mass Fraction (%)
6	C	27.43	7.63
8	O	6.75	2.5
27	Co	65.82	89.87

(b) Co-BTC@ZIF-67-C

Z	Element	Atomic Fraction (%)	Mass Fraction (%)
6	C	23.31	7.94
7	N	2.51	2.02
8	O	27.01	12.25
27	Co	47.16	78.81

(c) Nanowire@bubble-C

Z	Element	Atomic Fraction (%)	Mass Fraction (%)
6	C	56.72	23.57
7	N	1.14	0.55
8	O	6.77	3.75
27	Co	35.38	72.13

(d)

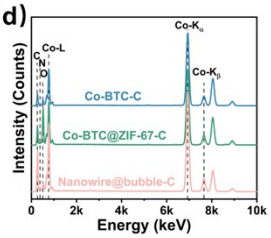

(e) Co-MOF-74-C

Z	Element	Atomic Fraction (%)	Mass Fraction (%)
6	C	21.46	8.12
8	O	39.90	20.12
27	Co	38.63	71.75

(f) Co-MOF-74@ZIF-67-C

Z	Element	Atomic Fraction (%)	Mass Fraction (%)
6	C	42.81	16.88
7	N	3.07	1.41
8	O	16.32	8.57
27	Co	37.80	73.14

(g) Nanorod@bubble-C

Z	Element	Atomic Fraction (%)	Mass Fraction (%)
6	C	51.93	22.32
7	N	1.98	0.99
8	O	13.37	7.66
27	Co	32.72	69.03

(h)

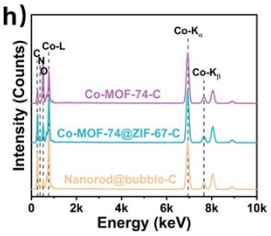

Figure S12. a–h) elemental–mapping analysis and corresponding EDX of all MOF derivatives.

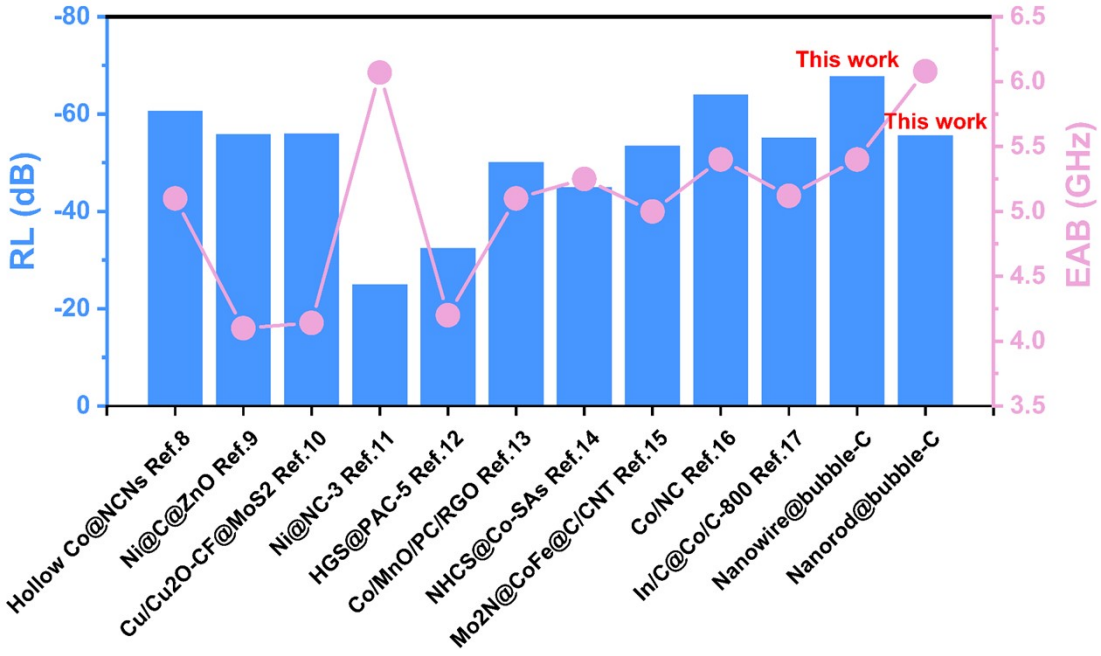

Figure S13. Comparison of electromagnetic wave absorption properties of previously reported similar carbon–based absorbers and this work.

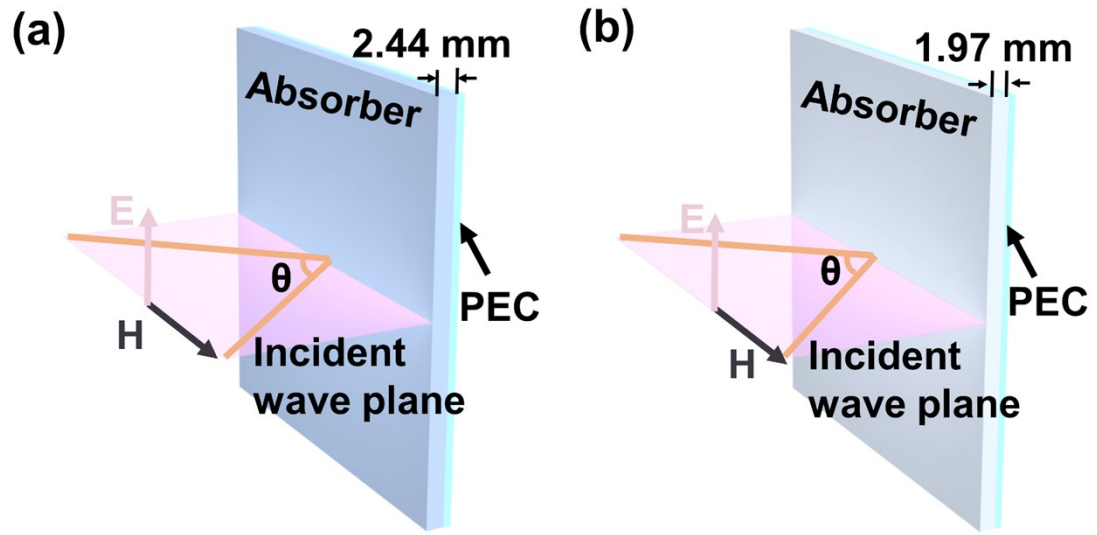

Figure S14. a) The model of Co–BTC–C, Co–BTC@ZIF–67–C, and Nanowire@bubble–C for RCS simulation at 9.4 GHz. b) The model of Co–MOF–74–C, Co–MOF–74@ZIF–67–C, and Nanorod@bubble–C for RCS simulation at 13.92 GHz.

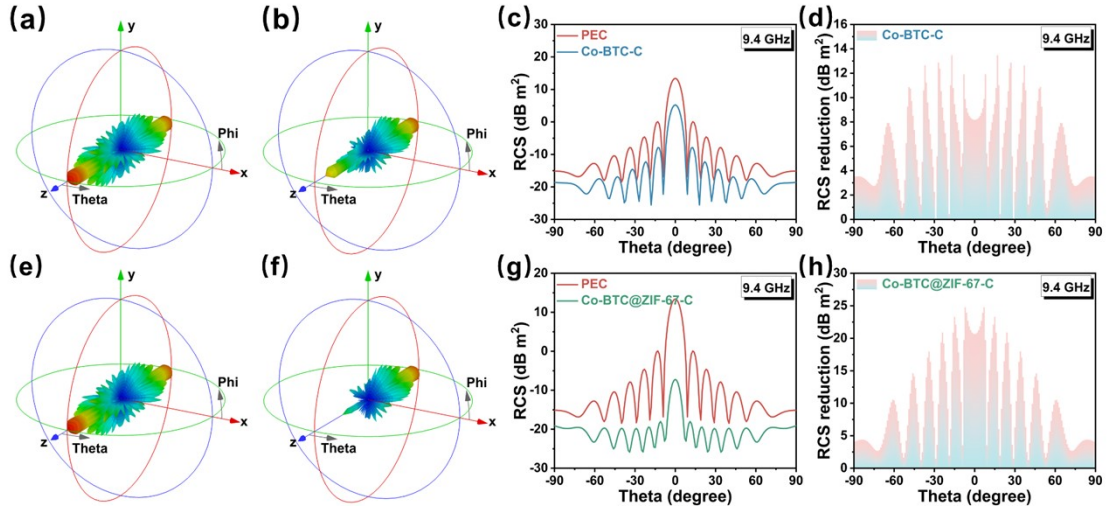

Figure S15. a, b) 3D RCS simulation plots, and c) RCS simulated curves of PEC and Co–BTC–C from different scanning angles. m) RCS reduction values of Co–BTC–C. e, f) 3D RCS simulation plots, and g) RCS simulated curves of PEC and Co–BTC@ZIF–67–C from different scanning angles. h) RCS reduction values of Co–BTC@ZIF–67–C.

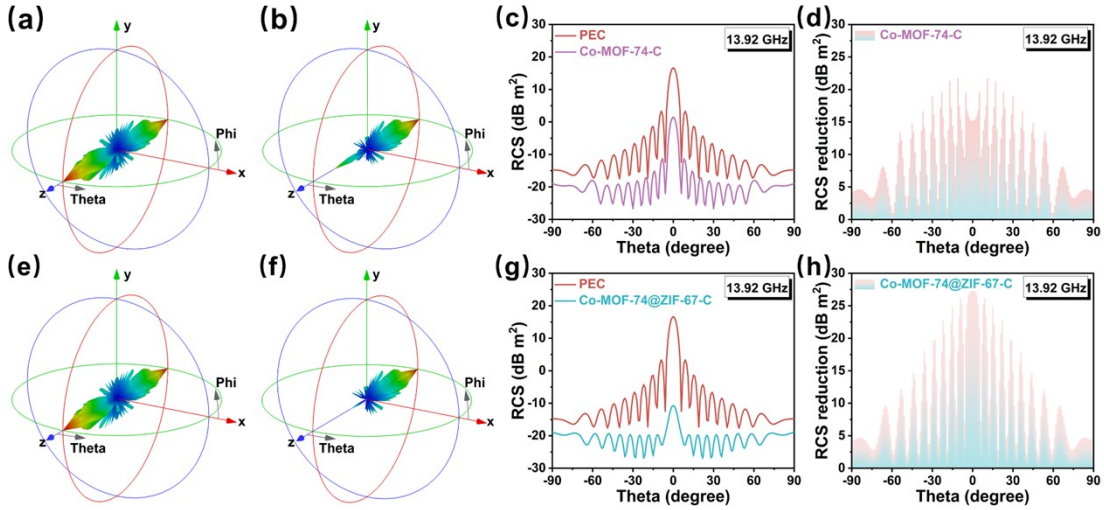

Figure S16. a, b) 3D RCS simulation plots, and c) RCS simulated curves of PEC and Co–MOF–74–C from different scanning angles. m) RCS reduction values of Co–MOF–74–C. e, f) 3D RCS simulation plots, and g) RCS simulated curves of PEC and Co–MOF–74@ZIF–67–C from different scanning angles. h) RCS reduction values of Co–MOF–74@ZIF–67–C.

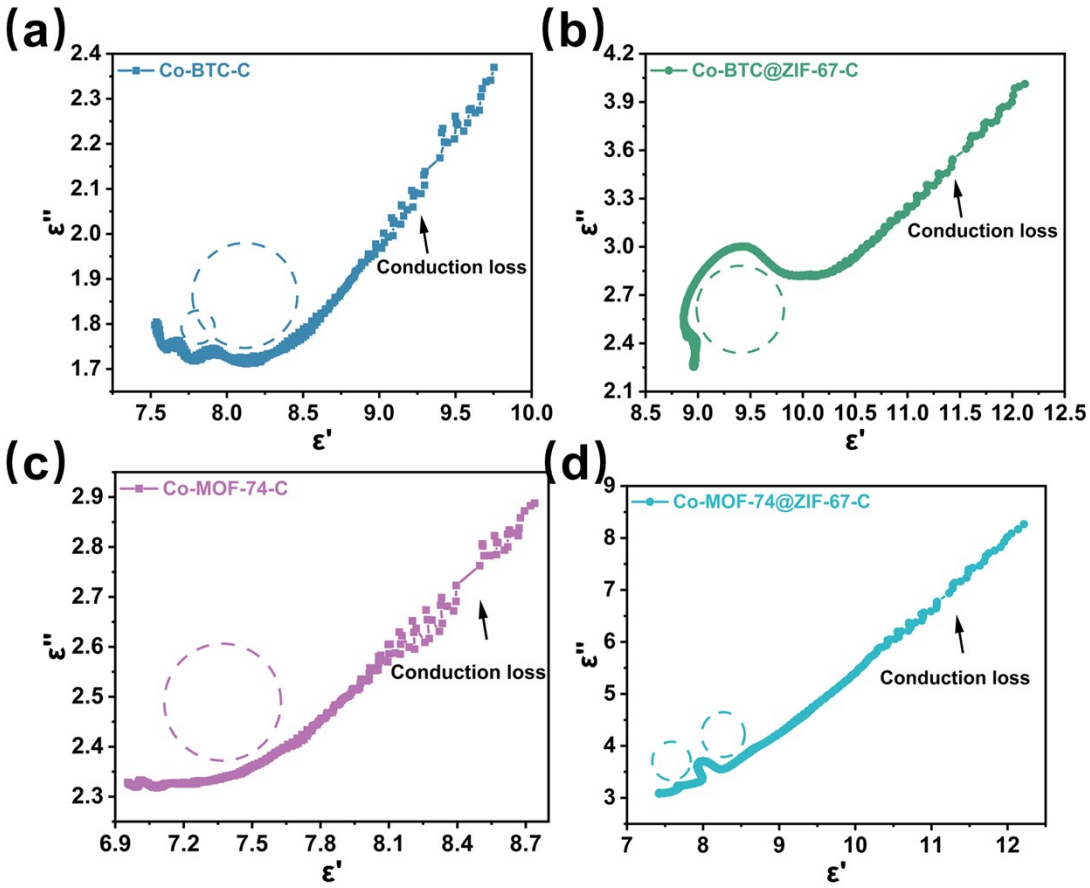

Figure S17. a–d) The Cole-Cole curves of Co–BTC–C, Co–BTC@ZIF–67–C, Co–MOF–74–C, and Co–MOF–74@ZIF–67–C.

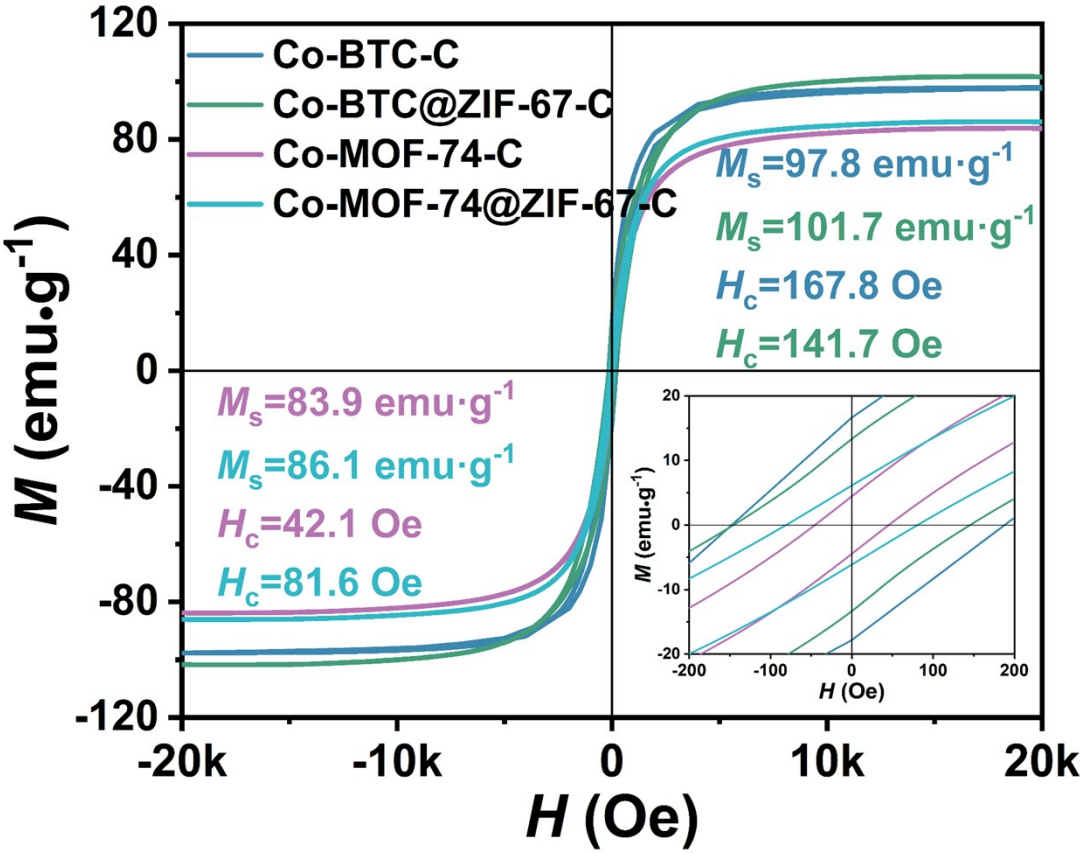

Figure S18. Hysteresis loops of Co–BTC–C, Co–BTC@ZIF–67–C, Co–MOF–74–C, Co–MOF–74@ZIF–67–C.

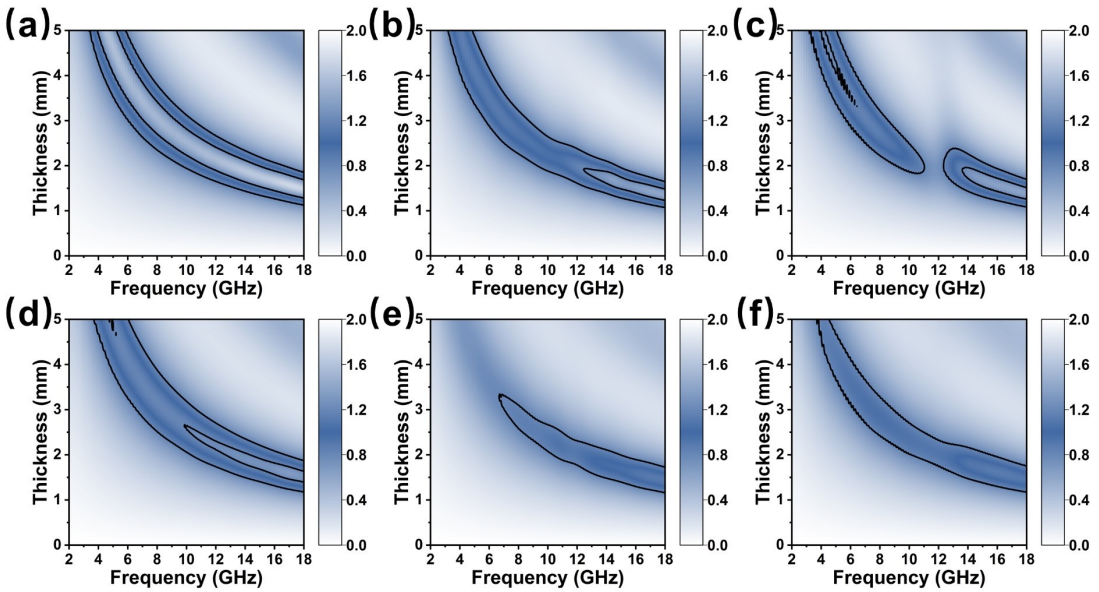

Figure S19. a–f) 2D contour maps $|Z_{in}/Z_0|$ of Co–BTC–C, Co–BTC@ZIF–67–C, Nanowire@bubble–C, Co–MOF–74–C, Co–MOF–74@ZIF–67–C, and Nanorod@bubble–C.

References

1. Y. Chen, Y. Wang, C. Li, W. Wang, X. Xue, H. Pan and R. Che, *Small*, 2024, 2401618.
2. C. Yu, D. Lin, J. Guo, K. Zhuang, Y. Yao, X. Zhang and X. Jiang, *Small*, 2024, 2401755.
3. Y. He, J. Zhou, J. Tao, X. Zhang, Z. Yao and X. Hao, *Chem. Eng. J.*, 2023, **472**, 144841.
4. Q. Liu, Q. Cao, H. Bi, C. Liang, K. Yuan, W. She, Y. Yang and R. Che, *Adv. Mater.*, 2015, **28**, 486-490.
5. Z. L. Hou, X. Gao, J. Zhang and G. Wang, *Carbon*, 2024, **222**, 118935.
6. Z. L. Hou, K. Du, Y. Zhang, S. Bi and J. Zhang, *Nano Res.*, 2022, **16**, 2604-2610.
7. R. Liu, Y. Wang, P. Wang, H. Kimura, B. Wang, C. Hou, X. Sun, W. Du and X. Xie, *Small*, 2024, 2402438.
8. P. Liu, S. Gao, G. Zhang, Y. Huang, W. You and R. Che, *Adv. Funct. Mater.*, 2021, **31**, 2102812.
9. L. Wang, X. Yu, X. Li, J. Zhang, M. Wang and R. Che, *Chem. Eng. J.*, 2020, **383**, 123099.
10. X. Zhao, Y. Huang, X. Liu, H. Jiang, M. Yu, X. Ma, M. Zong and P. Liu, *Chem. Eng. J.*, 2024, **483**, 149085.
11. Y. Liu, X. He, Y. Wang, Z. Cheng, Z. Yao, J. Zhou, Y. Zuo, R. Chen, Y. Lei, R. Tan and P. Chen, *Small*, 2023, **19**, 2302633.
12. H. Xu, X. Yin, M. Zhu, M. Li, H. Zhang, H. Wei, L. Zhang and L. Cheng, *Carbon*, 2019, **142**, 346-353.
13. J. Luo, X. Li, W. Yan, P. Shu and J. Mei, *Carbon*, 2023, **205**, 552-561.
14. B. Li, Z. Ma, J. Xu, X. Zhang, Y. Chen and C. Zhu, *Small*, 2023, **19**, 2301226.
15. C. Xu, L. Wang, X. Li, X. Qian, Z. Wu, W. You, K. Pei, G. Qin, Q. Zeng, Z. Yang, C. Jin and R. Che, *Nano-Micro Lett.*, 2021, **13**, 47.
16. Y. Zhou, P. He, W. Ma, P. Zuo, J. Xu, C. Tang and Q. Zhuang, *Small*, 2023, **20**, 2305277.

17. D. Fang, S. Liu, J. Li and H. Jin, *J. Alloys Compd*, 2023, **961**, 170992.